JOURNAL OF MATERIALS SCIENCE 28 (1993) 6466–6473

Influence of yttrium on microstructure and point defects in α-Al_2O_3 in relation to oxidation

M. K. LOUDJANI, A. M. HUNTZ
Laboratoire de Métallurgie Structurale, CNRS UA 1107, Université Paris XI, 91405 Orsay Cedex, France

R. CORTÈS
Laboratoire de Physique des Liquides et Electrochimie, CNRS GR4, Université Pierre et Marie Curie, 75230 Paris Cedex 05, France

Although the influence of yttrium on transport properties of α alumina has been the object of many studies, the mechanisms by which this element acts have not yet been elucidated. The method of modification by yttrium of the microstructure of α polycrystalline alumina and the nature of the point defects created by this doping element were studied. The results obtained are discussed in relation to alumina transport properties and especially in relation with the effect of yttrium on the oxidation mechanism of alumina former alloys, taking into account the doping amount.

1. Introduction

The beneficial effect of yttrium on the oxidation resistance of chromia or alumina former alloys has been known for many years [1, 2] and has been the object of numerous experimental works. Yttirium is known to decrease the oxidation kinetics in most cases, and especially to increase strongly the scale adherence. Attempts have been made in the last 10 years to elucidate the mechanisms by which yttrium acts. Better results were obtained in case of chromia scales than for alumina scales [3–6]. In alumina scales, various and sometimes opposite mechanisms have been suggested in order to explain the yttrium effect, particularly on transport properties. For example, according to the predominant diffusion (cationic or anionic diffusion) which ensures alumina scale growth, it is proposed that yttrium either decreases aluminum diffusion [7] or oxygen diffusion [8, 9], and in either case such an effect may be explained on the basis of the influence of yttrium on the cationic or anionic point defects.

In many cases attempts have been made to compare the effect of yttrium on growth of the alumina scale with the effect of yttrium on the transport properties of massive aluminas which has been the object of many studies [9–19]. In the case of conductivity or diffusion experiments, all authors agree that yttrium incorporated in alumina as a doping element acts as a "donor". But this observed effect has not been clearly explained and there is also a lack on experimental data on self-diffusion in alumina. The problem consists in the fact that yttrium is isoelectronic with aluminium and the "donor" effect is attributed to the large size of yttrium compared to aluminium without any explanation about the effect of yttrium on the nature of the point defects and their amount. Some studies also point out that yttrium has a strong tendency to segregate either along grain boundaries or at the surface of massive aluminas [16, 20], but the influence of such a phenomenon on the behaviour of the alumina scale has not been discussed.

In order to make a contribution to the understanding of the effect of yttrium on the high-temperature resistance of alumina former alloys, the microstructure and the local atomic structure of massive polycrystalline yttrium-doped aluminas were studied. Our objective consisted in clarifying the effect of yttrium doping on the microstructure of aluminas doped with variable amounts of Y_2O_3, in characterizing the grain-boundary segregation phenomena, and, particularly, in elucidating the influence of yttrium on the nature and the number of point defects in alumina in order to explain the "donor" effect of yttrium. For this last objective, a particularly sensitive technique, extended X-ray absorption fine structure (EXAFS) analyses, was used.

2. Materials and procedure

2.1. Materials

Massive undoped and Y_2O_3 doped α aluminas have been obtained by sintering-using the following powders.

(i) A 15Z alumina powder provided by "Rubis Synthétique des Alpes" (now Baïkowski Chimie) of 99.999 % purity and granulometry ~ 50 nm.

(ii) Yttria powder provided by "Rhône Poulenc, Chimie fine", of 99.99 % purity and granulometry ~ 100 nm.

Two doped aluminas have been produced with 0.1 and 0.03 mol %. The alumina powder was mixed with an yttrium nitrate solution [$Y(NO_3)_3 \cdot 6H_2O$] prepared from the yttria powder [21]. The mixed powders were then introduced into a borosilicate balloon,

0022–2461

for the 0.1% doped alumina, and into a polyethylene balloon, for the 0.03% doped alumina, placed in a boiler in order to eliminate the water. The obtained product was ground in a teflon crucible then calcined in a quartz tube for 48 h at 550 °C, first in a primary vacuum and secondly in oxygen. The product was again ground.

Sintering was performed by P. Carry Ecole Polytechnique de Lausanne, at 1550 °C for 15 min in a vacuum of 10^{-3} Pa under a uniaxial load of 45 MPa [16, 21]. The obtained pellets had a volumic mass equal to 3.98 $g\,cm^{-3}$, i.e. practically the theoretical value. Chemical analyses indicated that the procedure using a borosilicate balloon induced a silicon contamination.

Thin foils were prepared by mechanical polishing (up to $\sim$ 70 μm) then ionic sputtering (Laboratoire de Chimie du Solide, UPS Orsay). For transmission electron microscopy observations, the thin foils were covered with a thin carbon film.

2.2. Procedure

Alumina samples have been studied either as-sintered or heat treated between 1350 and 1650 °C in air.

SEM, TEM and STEM observations or analyses were performed. It must be noted that in SEM, back-scattered electrons offer the advantage of allowing yttrium detection due to its important atomic number compared to aluminium. Experiments were also made on a $FeC_{22}Al_5$ alloy which develops an alumina scale by oxidation, in order to compare the effect of yttrium on the microstructure of alumina obtained by sintering or by oxidation at high temperature. Yttrium was introduced by implantation by J. C. Pivin (CSNSM, Orsay), ($\sim$ 10% Y on 20 nm) and samples were oxidized at 1200 °C. If all the yttrium was incorporated in the scale, its concentration in alumina was about 0.13 mol %. Thin foils of the scale were then prepared.

The effect of yttrium on the point defects in massive aluminas was studied by EXAFS at Lure, Orsay. Details of this technique are given elsewhere [22–25]. Such experiments allow both the average distance, R_j, between the absorber atom (Y in our case) and the neighbouring atoms in the jth shell, and the average number, N_j, of diffusers (first, second, . . . , neighbours, in our case O, Al or Y) in the shell concerned, to be deduced. Analysis of the EXAFS experimental data also requires the use of standards: powders of Al_2O_3, Y_2O_3, $Y_3Al_5O_{12}$ and $YAlO_3$ [15, 24, 25]. Experiments were performed either in the transmission mode, on the standards, or in the fluorescence mode for the doped alumina samples.

3. Results

3.1. Microstructural study by SEM, TEM and STEM

Samples of undoped alumina, as-sintered or heat-treated in air at 1500 °C, were characterized by a grain size of $\sim$ 2–5 μm, with some grains lengthened in a direction perpendicular to the uniaxial load (Fig. 1a). The grain boundaries are particularly linear, indicating their purity [27]. After heat treatment at high temperature (for example, 1650 °C), it was observed that some grains became larger ($\sim$ 10 μm) (Fig. 1b). Porosities were never observed.

In the 0.1 mol % Y_2O_3-doped alumina samples, curved grain boundaries were observed associated with fairly equiaxed grains. The grain size was homogeneous and somewhat smaller than for undoped alumina (Fig. 2a). A precipitated phase made of $Y_3Al_5O_{12}$ appeared along the grain boundaries and in the bulk (white phase on back-scattered electron mode, Fig. 2a). After heat treatment at 1350 °C, some grain boundaries were locked by the intergranular precipitates (Fig. 2b), and the transgranular precipitates were surrounded by a dislocation network (Fig. 2c).

For the 0.03 mol % Y_2O_3-doped alumina samples, the $Y_3Al_5O_{12}$ phase was not observed, whatever the heat treatment (as-sintered or heat treated), indicating that the solubility limit of yttrium in a polycrystalline sample is $\geqslant$ 300 p.p.m. The grain size was homogeneous and equal to $\sim$ 3.5 μm. Statistical analyses of the L_α ray of yttrium have been performed along and perpendicular to the grain boundaries of thin foils, with an electronic probe of 80 nm. The apparent yttrium concentrations (obtained without calibration

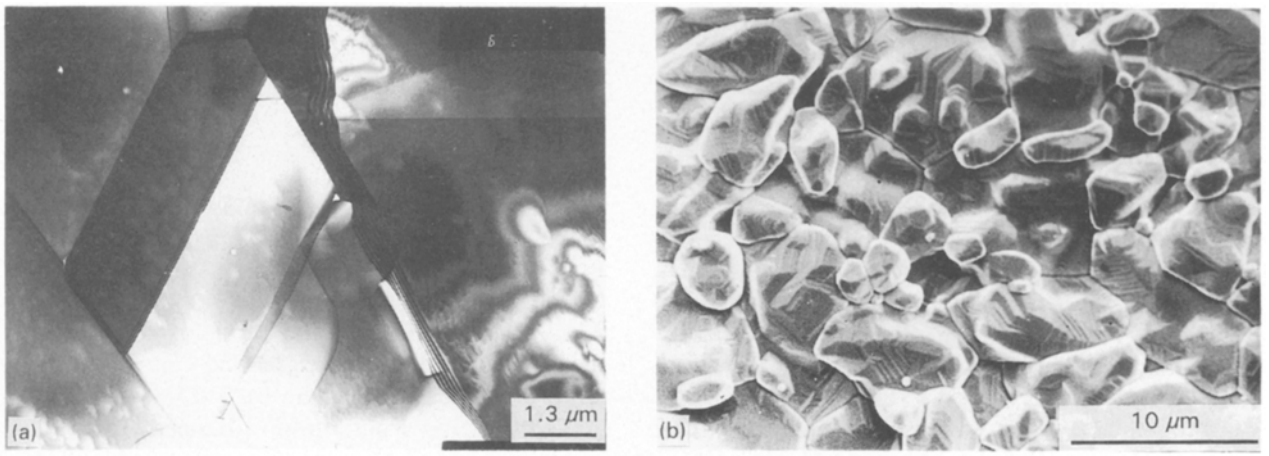

Figure 1 Microstructure of (a) as-sintered undoped alumina, (b) then heat-treated for 72 h at 1650 °C in air.

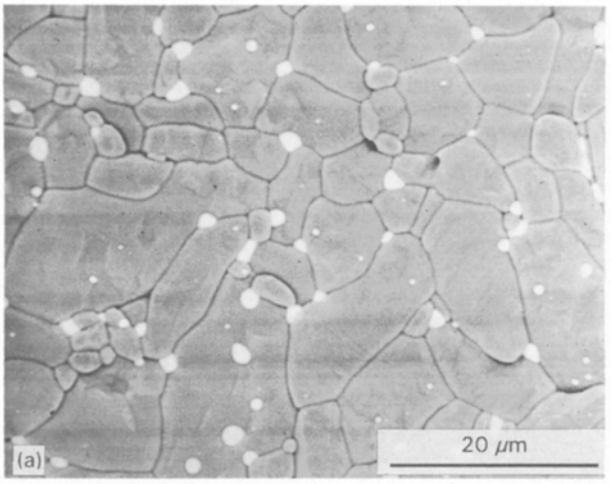

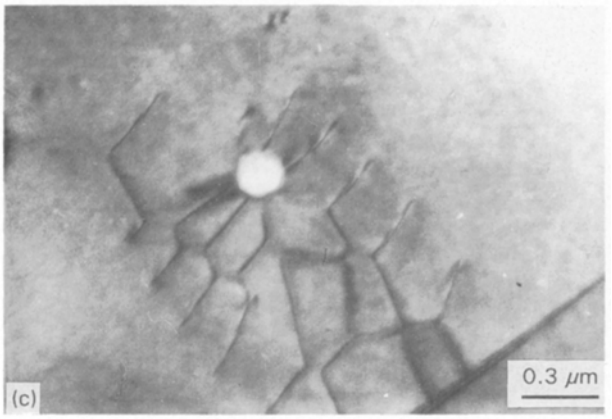

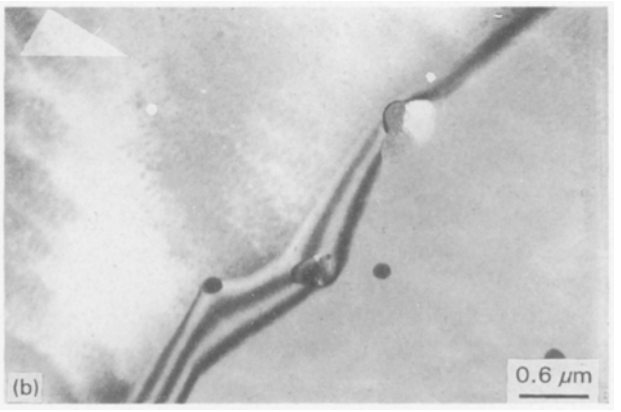

Figure 2 Microstructure of 0.1 mol % Y_2O_3 doped alumina, (a) after heat treatment for 72 h at 1650 °C in air, (b–c) after heat treatment for 24 h at 1350 °C in air.

with a standard) were $C_b \sim 0.4$–0.5 at % and $C_{gb} \sim 0.8$ at % in the bulk and in grain boundaries, respectively, but it is clear that the concentration obtained along grain boundaries was apparent because it takes into account contributions from the boundary and from a part of the bulk due to the probe size. This will be discussed later.

The alumina thin foils obtained from the oxidized yttrium-doped FeCrAl alloy had a grain size (diameter $\simeq 0.3$ μm) smaller than that of massive aluminas (Fig. 3). The grain morphology was regular and some precipitates enriched in yttrium were observed along grain boundaries and in the bulk of the grains. This is consistent with the expected value for the yttrium concentration in the scale (0.13 mol % if all implanted yttrium is incorporated in to the scale after oxidation).

3.2. Chemical state of yttrium in alumina and point defects

Figs 4 and 5 show the Fourier-transform magnitude spectrum (uncorrected for phase shift) obtained on as-sintered 0.1 and 0.03 mol % Y_2O_3 doped aluminas, respectively. On these curves, the peak position is representative (phase factor apart), of the distances R_j and the peak surface is proportional to the neighbouring atom number, N_j, on the jth shell.

As a first step, it is necessary to compare these spectra with those of the standards, Al_2O_3, $Y_3Al_5O_{12}$, Y_2O_3 and $YAlO_3$, (Figs 6 and 7). Such a comparison

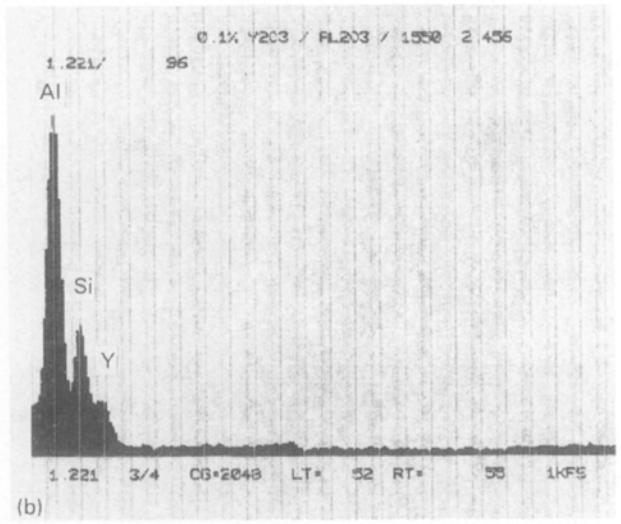

Figure 3 (a) Microstructure of the thermal alumina doped in yttrium, and (b) the EDAX spectrum.

indicates [16, 25, 26] that in the sample doped with 0.1 mol % Y_2O_3, most of the yttrium is precipitated in the $Y_3Al_5O_{12}$ phase (cf. Figs 4 and 7a), while for the sample doped with 0.03 mol % Y_2O_3 the spectrum notably differs from those obtained for Y_2O_3, $Y_3Al_5O_{12}$ and $YAlO_3$ compounds (cf. Figs 5 and 7a, b, c). However, an analogy in the peak position

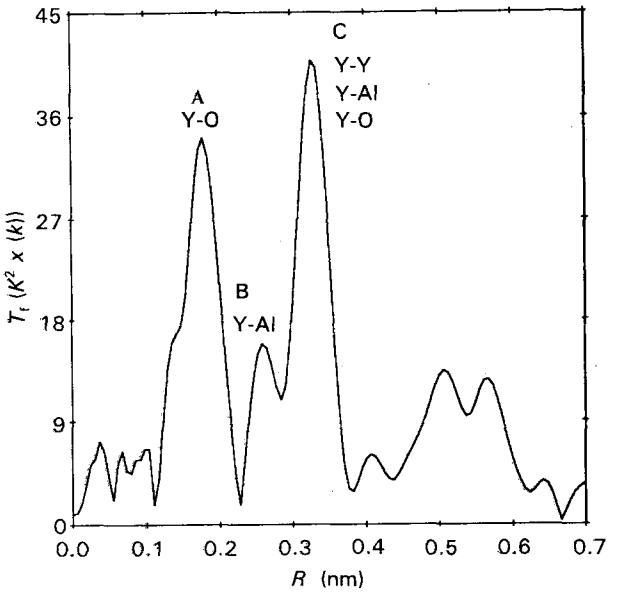

Figure 4 Fourier-transform magnitude spectrum (uncorrected for phase shift) of 0.1 mol % Y_2O_3-doped alumina.

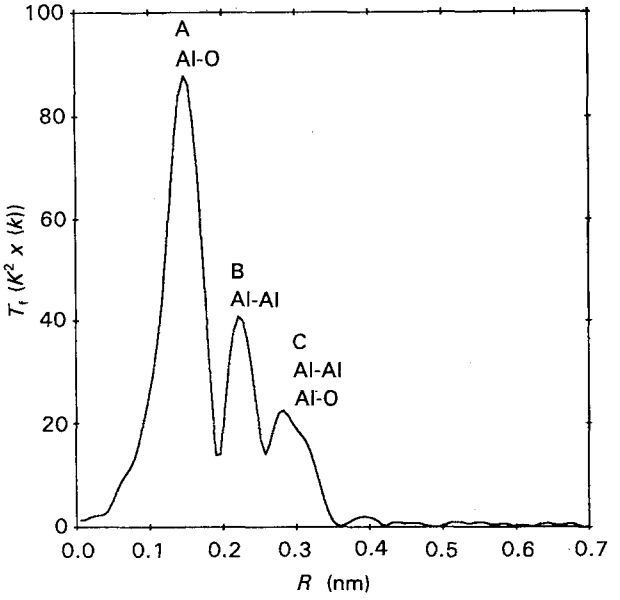

Figure 6 Fourier-transform magnitude spectrum (uncorrected for phase shift) of Al_2O_3.

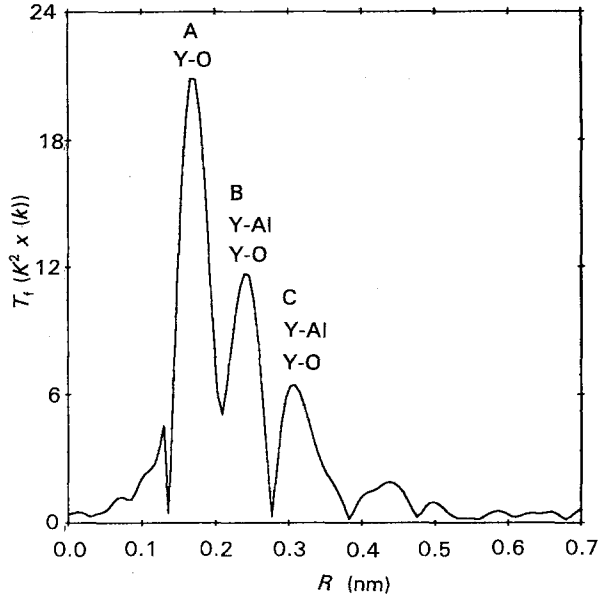

Figure 5 Fourier-transform magnitude spectrum (uncorrected for phase shift) of 0.03 mol % Y_2O_3-doped alumina.

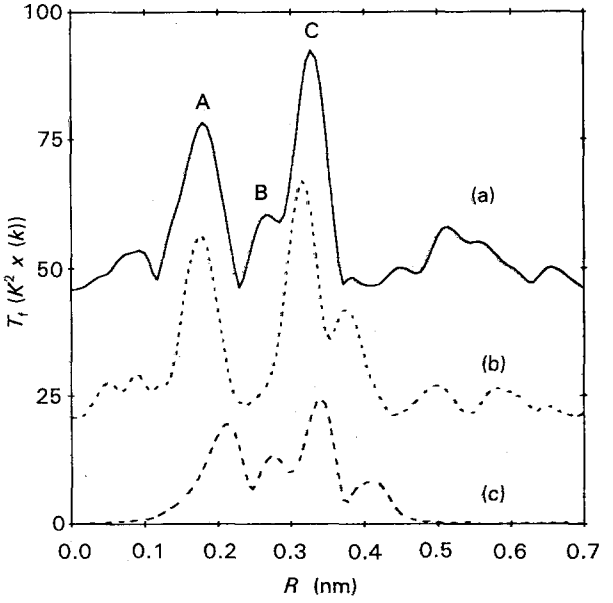

Figure 7 Fourier-transform magnitude spectra (uncorrected for phase shift) of (a) $Y_3Al_5O_{12}$, (b) Y_2O_3, (c) $YAlO_3$.

appears between the spectrum of the 0.03 mol % Y_2O_3-doped alumina (Fig. 5) and that obtained with alumina (Fig. 6). As the peak amplitude in these two figures is different, a second alumina spectrum was established by taking into account the fact that yttrium ions, whose size is largely greater than aluminium ions ($R_{Y^{3+}} = 0.092$ nm and $R_{Al^{3+}} = 0.054$ nm), are located on aluminium sites (Fig. 8b), and by considering the experimental N_j values. Then, the Fourier-transformed spectra of such a calculated structure (Fig. 8b) and of the 0.03 mol % Y_2O_3-doped alumina (Fig. 8a) are similar.

From these Fourier transformed spectra, the values of N_j and R_j in the doped alumina samples have been determined and compared with the values calculated for the standards (Tables I–III).

In the case of the alumina doped with 0.1 mol % Y_2O_3, the comparison of the spectra (Figs 4 and 7a) and of the N_j and R_j values (Table I) clearly indicates that most of the yttrium is precipitated as $Y_3Al_5O_{12}$ phase. This agrees with the microstructural observations by TEM and STEM.

For the alumina doped with 0.03 mol % Y_2O_3, a comparison of its spectrum (Fig. 5) with those of the standards (Figs 6–8) has shown that the structrure was only consistent with an alumina structure where yttrium ions are located on aluminium sites. In Table II, the values of N_j and R_j deduced from the experimental spectrum of the 0.03% doped sample are reported. They can be compared to the distances Y_{Al}–O and Y_{Al} – Al in alumina and to the values of N_j calculated without taking into account a size effect

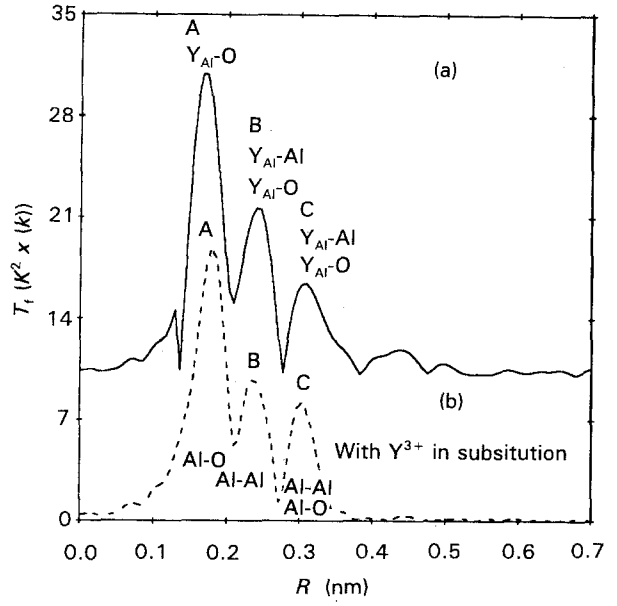

Figure 8 Fourier-transform magnitude spectrum (uncorrected for phase shift) of (a) 0.03 mol % Y_2O_3-doped alumina, and (b) Al_2O_3 calculated by considering that big yttrium ions are in substitution on aluminium ion sites.

TABLE I Fit of the parameters R_j (nm), N_j determined for the 0.1 mol % Y_2O_3 doped polycrystalline α-alumina. Comparison with the same parameters calculated in $Y_3Al_5O_{12}$ from peaks A–C of Fig. 4

Peak	Samples	Neighbours	$\bar{R}_j$ (nm) ± 0.008	$\bar{N}_j \pm 0.5$
A	0.1% mol Y_2O_3	Peak A ⟨Y–O⟩	0.238	8.3
	$Y_3Al_5O_{12}$	Peak A ⟨Y–O⟩	0.2369	8
B, C	0.1% mol Y_2O_3	Peak B Y–Al1	0.303	1.9
		Peak B Y–Al2	0.332	6.2
		Peak C Y–Al3	0.366	4.4
		Peak C Y–Y	0.371	3.2
		Peak C Y–O	0.390	5.2
	$Y_3Al_5O_{12}$	Peak B Y–Al1	0.3003	2
		Peak B Y–Al2	0.3357	4
		Peak C Y–Al3	0.3677	4
		Peak C Y–Y	0.3677	4
		Peak C Y–O	0.3876	8

(Table III). For the first shell, the experimental Y_{Al}–O distance is greater than the calculated Y_{Al}–O distance and the experimental value of N_j is smaller than the calculated value. For the second shell, the Y_{Al}–Al distance is similar for both experimental and calculated cases. A third shell made of oxygen ions appears in the experimental case located at half the distance between the two successive oxygen shells in alumina. This suggests that in 0.03 mol % Y_2O_3-doped alumina there is an oxygen shell in the interstitial position due to the large size of the yttrium ions. The average Y–O distances have been calculated from the ionic radii of Y^{3+} and O^{2-} according to the site symmetry of each ion [16, 25, 28, 29]. The Y_{Al}–O distance determined from the 0.03% doped sample, 0.232 nm, is consistent with an octahedral symmetry for yttrium ions: in this case $R_{O^{2-}} = 0.140$ nm and $R_{Y^{3+}} = 0.092$ nm. This is in agreement with the fact that yttrium substitutes for aluminium. As yttrium

TABLE II Fit of the parameters R_j(nm), N_j determined from peaks A and B for the 0.03 mol % Y_2O_3 doped polycrystalline α-alumina (Fig. 5)

Peaks	Neighbours	$\bar{R}_j$ (nm) ± 0.08	$\bar{N}_j$
A	Y–O	0.232	2.7 ± 0.5
B	Y–Al	0.274	2.6 ± 1
B	Y–O	0.285	1.7 ± 1

TABLE III Theoretical distances Y_{Al}–O and Y_{Al}–Al in alumina (Fig. 6) and values of N_j calculated without taking into account a size effect

Peaks	Neighbours	R_j (nm) ± 0.08	N_j
A	Y_{Al}–O	0.1912	6
B	Y_{Al}–Al	0.2755	4
C	Y_{Al}–Al	0.3403	9
C	Y_{Al}–O	0.3405	9

ions are larger than aluminium ions, the coordinance number, R_j, decreases from 6 to ~ 3 (cf. Tables II and III) which indicates that oxygen vacancies are created in the alumina lattice and induce a displacement of other oxygen atoms (in interstitial positions).

It must be remarked that EXAFS analyses are relative to yttrium located in the bulk and that yttrium segregated in the grain boundaries does not contribute to the EXAFS signal. This will be discussed later.

4. Discussion

From microstructural observations and EXAFS analyses, it appears that the influence of yttrium in alumina depends on its amount.

For Y_2O_3 amounts greater than ~ 0.03 mol %, most of the doping element is precipitated as $Y_3Al_5O_{12}$ in the bulk and along grain boundaries. These precipitates stabilize the alumina grain size by locking the grain boundaries. The main action of this doping element will consist in modifying the "short circuit" diffusion phenomena (intergranular and interphase diffusion) owing to the creation of new and different interfaces. Nevertheless, in such cases, a small part of the yttrium must be in solid solution, as suggested by the shoulder observed on peak A of Fig. 4. This type of yttrium will have the same effect as that discussed for the 0.03 mol % Y_2O_3-doped alumina later. It must be kept in mind also that in addition to the effect on diffusion phenomena, the doping element will act on creep properties of alumina scales because it decreases the grain size compared to undoped alumina. During oxidation of alumina former alloys, if an important amount of yttrium ($\geqslant$ 300 p.p.m.) is incorporated in the alumina scale, it can be suggested that the predominant effect will be related to the presence of segregated or precipitated yttrium along grain boundaries and to the microstructural modifications. The creep properties of the scale should be improved owing to the grain size decrease, and the short-circuit diffusion should be modified.

For Y_2O_3 amounts equal to ~ 0.03 mol %, yttrium is dissolved and is either localized by substitution into aluminium ions in the bulk or segregated in grain boundaries. The apparent solubility of yttrium is ~ 300 p.p.m. for the production conditions of this study, i.e. $T = 1550\,°C$ and low oxygen pressure. But yttrium atoms segregate in the grain boundaries and it was found that the average apparent molar (Y_2O_3) concentration in the bulk and in grain boundaries was equal to $C_b \sim 0.45\%$ mol and $C_{gb} \sim 0.80\%$ mol respectively.

If the grain boundary volumic fraction in the analysed area is noted, f_{gb}, the apparent concentration determined along the boundary, C_{gb}, is related to the probe size, Φ, and to the grain boundary width, δ, and is equal to

$$C_{gb} = f_{gb} C_{GB} + (1 - f_{gb}) C_B \quad (1)$$

with C_{GB} the real concentration in the grain boundary and C_B the real contribution of the bulk.

As $\delta \ll \Phi$, it can be assumed $C_B \sim C_b$, then

$$C_{GB} = [C_{gb} - (1 - f_{gb}) C_b]/f_{gb} \quad (2)$$

In our case, $f_{gb} = [(\delta\Phi x)/(\pi\Phi^2 x/4)]$, with x the thin foil thickness. So, the ratio of the yttrium concentration in the grain boundary to that in the bulk is $C_{GB}/C_b \sim 50$ (with $\delta = 1$ nm and $\Phi = 80$ nm), indicating that the actual yttrium concentration in the grain boundary is 50 times greater than in the bulk.

As the average concentrations in the polycrystal c_b and c_{GB} obey Equation 3 (if a model of cubic grains is applied)

$$(1 - 3\delta/G)c_b + (3\delta/G)c_{GB} = 300_{\text{p.p.m. mol}}\ Y_2O_3 \quad (3)$$

with G the alumina grain size ($\sim 3.5 \times 10^3$ nm) and $3\delta/G$ the volume fraction of grain boundaries per unit volume of polycrystalline material, the average bulk concentration can be calculated and is found to be $c_b = 288$ p.p.m. mol Y_2O_3 (assuming $c_{GB}/c_b = C_{GB}/C_b$). Per unit volume of polycrystalline material, there are ~ 12 p.p.m. mol Y_2O_3 in the grain boundaries. Thus the EXAFS signal is mainly due to yttrium present in the bulk. The contribution of yttrium in grain boundaries to the signal is equal to 12/288, $\sim 4\%$. It also confirms that the apparent solubility limit of yttrium in polycrystalline alumina is near 300 p.p.m. mol Y_2O_3. It it is assumed that the 0.03 mol % Y_2O_3-doped alumina is homogeneous at the grain scale, the real solubility limit of yttrium in the bulk of a single crystal can be calculated according to $C_b + C_{GB} = 300$ p.p.m. mol Y_2O_3 and $C_{GB}/C_b \sim 50$, so the deduced real concentration in the bulk of a single crystal is $C_b \sim 6$ p.p.m. mol Y_2O_3.

The effect of yttrium in solid solution on the point defects and on the transport properties of alumina were then investigated. From EXAFS results, it appears that yttrium is localized on aluminium sites. Owing to its large size, it induces the creation of oxygen vacancies, $V_O^{\bullet\bullet}$ (on the first neighbouring shell) and of oxygen interstitials, O_i'', on a second shell. Thus yttrium induces a localized point defect complex according to the following equation

TABLE IV Ionization energy of Y^{3+} and O^{2-} ions

	Atomic orbitals		Atomic orbitals	
	$2P_{1/2}$	$2P_{3/2}$	$4P_{1/2}$	$4P_{3/2}$
Oxygen	6.6			
Yttrium			45.6	25.6
Reaction energy	$O^{2-} \rightarrow O^- + e^-$			9 eV

$$2Y_{Al}^x + 3O_O^x \rightleftharpoons 2Y_{Al}^x + V_O^{\bullet\bullet} + O_i'' \quad (3)$$

Many authors working on transport properties of alumina (conductivity, diffusion, etc.) [9–20, 30] found that yttrium acts as a donor for alumina. As yttrium is isoelectronic with aluminium, this effect is attributed to its large size ($\sim$ twice that of aluminium ions: 0.092 and 0.054 nm, respectively). Owing to the stable electronic configuration of Y^{3+} ions ([Ar] $3d^{10}\,4s^2\,4p^6$), and to the great ionization energy of the Y^{3+} ion compared to that of O^{2-} ions whose electronic configuration is [He] $2s^2\,2p^6$ (cf. Table IV), it seems more probable that the species responsible for the donor effect is oxygen ions, either on a lattice site or in an interstitial site. For steric reasons, the oxygen ionization seems more favourable for oxygen in the interstitial position. According to the point defect equation deduced from EXAFS experiments, it can be suggested that the donor effect is related to the following reaction

$$2Y_{Al}^x + 3O_O^x \rightleftharpoons 2Y_{Al}^x + 3V_O^{\bullet\bullet} + 3O_i' + e' \quad (4)$$

The defect complex can be noted $C = (2Y_{Al}^x + 3O_O^x)$ and it acts as a donor.

Thus, for high oxygen pressure, when the predominant alumina point defect is the aluminium vacancy V_{Al}''', the defect equation with a donor is [16]

$$3/4\ O_2 + 3C \rightleftharpoons 3C^{\bullet} + V_{Al}''' + 3/2O_O^x \quad (5)$$

because

$3[V_{Al}'''] = [C^{\bullet}]$, we obtain

$$[V_{Al}'''] \alpha [C]^{3/4} (pO_2)^{3/16} \quad (6)$$

Equation 6 indicates that the concentration of V_{Al}''' will increase with the complex defect amount, i.e. with the yttrium concentration, but its variation law with the oxygen pressure is not modified compared to undoped alumina. A similar behaviour will be obtained if it is considered that oxygen interstitials are the predominant defects in alumina: $[O_i']$ or $[O_i'']$ concentration increases with the doping element amount.

For low oxygen pressure, if the predominant alumina point defect is the aluminium interstitial $Al_i^{\bullet\bullet\bullet}$, then the effect of the donor will lead to [16]

$$3/4\ O_2 + Al_i^{\bullet\bullet\bullet} + 3C \rightleftharpoons 3C^{\bullet} + Al_{Al}^x + 3/2O_O^x \quad (7)$$

which indicates that the interstitial aluminium concentration will decrease with the donor defect complex amount. The same result is obtained with oxygen

vacancies according to the equation

$$1/2\,O_2 + V_O^{\bullet\bullet} + 2C \rightleftharpoons O_O^x + 2C^{\bullet} \quad (8)$$

From these considerations, it can be deduced that the transport properties of alumina will be modified by the presence of yttrium in solid solution.

Cationic diffusion, if it occurs by aluminium vacancies, must be enhanced by yttrium, and inversely if the cationic diffusion occurs by aluminium interstitials. In oxide scales made of alumina, when cationic diffusion is suggested to be the major transport process [31, 32], it is thought that cations diffuse by aluminium vacancies, because calculations [33] indicate that Schottky disorder is more probable than Frenkel disorder. Thus, it would be expected that yttrium increases the growth rate of alumina scale, provided that yttrium is localized in the outer part of the scale and that its effect is not counterbalanced by other impurities. This is consistent with the fact that in such a case, new oxide layers develop at the outer interface whose oxygen pressure is important. Indeed, in some cases, a growth-rate enhancement is observed [34].

For anionic diffusion via vacancies, yttrium in solid solution must decrease the diffusion rate as shown by Equation 8 and also because the oxygen vacancies created in the defect complex (Equation 3) are trapped by yttrium due to its large size. If anionic diffusion occurs by interstitial oxygen, then the anionic diffusion would be enhanced. Recent results concerning anionic self-diffusion in yttrium-doped alumina [35, 36] provide evidence of a slight enhancement of oxygen bulk diffusion due to yttrium, but grain-boundary diffusion is decreased. This must be due to grain-boundary segregation of yttrium. It is tempting to assume that anionic diffusion occurs by vacancies in grain boundaries and by interstitial oxygens in the bulk. In oxide scales whose growth seems to be controlled by oxygen diffusion [7, 37, 38], it is generally observed that yttrium decreases the oxidation rate, which suggests that anionic diffusion occurs preferentially by oxygen vacancies. This is consistent with the fact that in such cases new oxide layers develop at the inner interface whose oxygen pressure is small.

The microstructure modifications will also, even for low doping amounts, have an effect on the alumina scale properties. As shown in scales developed on doped FeCrAl alloy (Fig. 3), the grain size is decreased compared to undoped alumina and yttrium segregates and precipitates at the grain boundaries, which will probably induce greater strain abilities and a residual stress level somewhat lower than in undoped alumina scales.

5. Conclusions

The main conclusions that can be drawn from these structural (EXAFS) and microstructural (TEM and STEM) studies on massive undoped or yttrium-doped aluminas are as follows

1. The apparent solubility of yttrium in polycrystalline alumina is about 300 p.p.m. while, owing to yttrium segregation in the grain boundaries, the yttrium solubility in the bulk of a single crystal is about 6 p.p.m.

2. For samples with 300 p.p.m. mol Y_2O_3, yttrium is precipitated as $Y_3Al_5O_{12}$ which induces a decrease in the grain size, increases the creep abilities and modifies the short-circuit diffusion phenomena.

3. For samples with $\leqslant 300$ p.p.m. Y_2O_3, most of the yttrium (~ 288 p.p.m.) is in solid solution in the grains of the polycrystals. Yttrium ions are localized on aluminium sites and, due to its great size, induce a point defect complex made of oxygen vacancies (first neighbouring shell) and oxygen interstitials (second neighbouring shell). The donor effect of yttrium as a doping element must be due to oxygen ionization according to

$$2Y_{Al}^x + 3O_O^x \rightleftharpoons 2Y_{Al}^x + 3V_O^{\bullet\bullet} + 3O_i' + e'$$

4. According to these defects equations, it appears that yttrium will probably increase cationic diffusion by aluminium vacancies and decrease anionic diffusion by oxygen vacancies. However, the opposite effects will be observed if aluminium interstitials or oxygen interstitials are the predominant point defects in alumina.

If growth of alumina scales occurs predominantly by cationic diffusion at the outer interface of the scale, i.e. at high oxygen pressure, it is tempting to assume that yttrium (if localized in the outer part of the scale), will increase the growth rate of the alumina scale. If alumina scale growth occurs predominantly by oxygen diffusion at the inner part of the scale, i.e. at low oxygen pressure, the effect of yttrium (if localized in the inner part of the scale), will be to decrease the oxygen vacancy concentration and to decrease the oxidation rate. These apparently opposite effects could correspond to the fact that in some cases, authors find that yttrium doping increases the growth rate, or inversely. This is probably due to the fact that self-diffusion coefficients of oxygen and aluminium in "pure" alumina differ only slightly [34], and due to the impurities incorporated in the alumina scale according to the alloy purity and composition, oxygen or aluminium diffusion becomes predominant.

Simultaneously, yttrium doping will have an effect on the creep properties of the scale due to the grain-size decrease.

Acknowledgements

The authors thank C. Haut (Laboratoire de Métallurgie Structural, CNRS), for his help in SEM and STEM observations.

References

1. L. B. PFEIL, UK Pat. 459 848 (1937).
2. D. P. WHITTLE and J. STRINGER, *Phil. Trans. R. Soc. Lond. A* **295** (1980) 309.
3. F. H. STOTT and G. C. WOOD, *Mater. Sci. Eng.* **87** (1987) 267.
4. M. J. BENNET and D. P. MOON, in "The role of metals active elements in the oxidation behaviour of high temperature metals and alloys", edited by E. Lang (Elsevier Applied Science, 1989) p. 111.

5. A. M. HUNTZ, *ibid.*, p. 81.
6. J. JEDLINSKI, *Solid State Phenom.* **21/22** (1992) 335.
7. K. P. R. REDDY, J. L. SMIALEK and A. R. COOPER, *Oxid. Metals* **17** (1982) 429.
8. E. W. A. YOUNG and J. H. W. DE WIT, *Solid State Ionics* **16** (1985) 39.
9. *Idem, Oxid. Metals* **26** (1986) 351.
10. S. K. TIKU and F. A. KRÖGER, *J. Am. Ceram. Soc.* **63** (1980) 31.
11. M. M. EL-AIAT and F. A. KRÖGER, *ibid.* **65** (1982) 162.
12. H. A. WANG and F. A. KRÖGER, *ibid.* **63** (1980) 613.
13. M. LOUDJANI, B. LESAGE, G. PETOT-ERVAS, D. DEWERDEIR and A. M. HUNTZ, *Adv. Ceram.* **23** (1987) 125.
14. B. LESAGE, Doctor Thesis, University Paris XI, Orsay, France (1984).
15. D. PROT, Thesis, University Paris VI, France (1991).
16. M. K. LOUDJANI, Doctor Thesis, University Paris XI, Orsay, France (1992).
17. M. H. LAGRANGE, A. M. HUNTZ and J. Y. LAVAL, *Ann. Chim. Fr.* **12** (1987) 9.
18. K. KITAZAWA and R. L. COBLE, *J. Am. Ceram. Soc.* **57** (1974) 250.
19. M. DECHAMPS and F. BARBIER, in "Science of ceramics interfaces", edited by J. Nowotny (Elsevier Science, 1991) pp. 323–69.
20. G. PETOT-ERVAS, C. MONTY, D. PROT, C. SÉVERAC and C. PETOT, in "Structural Ceramics Processing, Microstructure and Properties", Proceedings of the 11th RISΦ International Symposium on Metallurgy and Materials Science, edited by J. J. Bentzen, J. B. Sorensen *et al.*, RISΦ National Laboratory, Denmark (1990) pp. 465–470.
21. M. K. LOUDJANI, B. LESAGE and A. M. HUNTZ, *l'Ind. Céram.* **801** (1986) 53.
22. D. E. SAYERS, E. W. LYTLE and E. A. STERN, *Phys. Rev. Lett.* **27** (1975) 4836.
23. F. W. LYTLE, D. E. SAYERS and E. A. STERN, *Phys. Rev. B* **11** (1975) 4825.
24. J. JAKLEVIC, J. A. KIRBY, M. P. KLEIN, A. S. ROBERTSON, G. S. BROWN and P. EISENBERGER, *Solid State Commun.* **23** (1977) 679.
25. M. K. LOUDJANI, R. CORTÈS, *J. Eur. Ceram. Soc.*
26. M. K. LOUDJANI, J. ROY, A. M. HUNTZ and R. CORTÈS, *J. Am. Ceram. Soc.* **68** (1985) 559.
27. S. LARTIGUE, Thesis, University of Paris XI, Orsay, France (1988).
28. L. PAULING, in " the Nature of Chemical Bond", 3rd Edn (Cornel University Press, 1960).
29. E. J. W. WHITTACKER and R. MUNTUS, *Geochem. Cosmochem. Acta* **34** (1970) 945.
30. F. A. KRÖGER, *Solid State Ionics* **12** (1984) 189.
31. A. M. HUNTZ, G. BEN ABDERRAZIK, G. MOULIN, E. W. A. YOUNG and J. H. W. DE WIT, *Appl. Surf. Sci.* **28** (1987) 345.
32. *Idem, Solid State Ionics* **22** (1987) 285.
33. G. J. DIENES, D. O. WELCH, C. R. FISHER, R. D. HATCHER, D. LAZARETH and M. SAMBERG, *Phys. Rev.* **B11** (1975) 3060.
34. R. PRESCOTT, D. F. MITCHELL, J. W. FRASER and M. J. GRAHAM, in "Proceedings of the 3rd International Symposium on High Temperature Corrosion and Protection of Materials", Les Embiez, 25–29 May 1992, to be published in *J. Phys.*
35. M. LE GALL, B. LESAGE, M. MILOCHE, A. M. HUNTZ and C. MONTY, in "Proceedings of the 6th International Conference on Intergranular and Interphase Boundaries in Materials", Thessaloniki, Greece, 22–26 June 1992.
36. M. LE GALL, Thesis, University Paris XI, France (1992).
37. T. A. RAMANARAYANAN, M. RACHAVAN and R. PETKOVIC-LUTON, *Oxid. Met.* **22** (1984) 83.
38. *Idem, J. Electrochem. Soc.* **131** (1984) 923.

Received 26 February
and accepted 27 April 1993